Applied Surface Science 707 (2025) 163654

Contents lists available at ScienceDirect

Applied Surface Science

journal homepage: www.elsevier.com/locate/apsusc

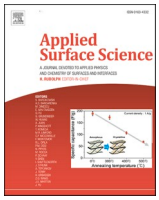

Full Length Article

Heterogeneous surface recombination of oxygen atoms on vertically oriented multilayer graphene sheets deposited on a metal substrate

Domen Paul [a,*], Miran Mozetič [a], Gregor Primc [a], Alenka Vesel [a], Sandra Drev [b], Rok Zaplotnik [a]

[a] Jožef Stefan Institute, Department of Surface Engineering, Teslova ulica 30, 1000 Ljubljana, Slovenia
[b] Jožef Stefan Institute, Center for Electron Microscopy and Microanalysis, Jamova cesta 39, 1000 Ljubljana, Slovenia

ARTICLE INFO

Keywords:
Plasma
Carbon nanowalls
Oxygen
Chemical vapor deposition
Recombination coefficient
Heterogeneous surface recombination

ABSTRACT

The kinetics of surface recombination of neutral oxygen atoms on nanocarbon deposited on oxidized cobalt catalyst in inductively coupled radiofrequency plasma sustained in propane in the H-mode is presented. The coefficient was measured in the range of temperatures between 300 and 800 K and pressures between 40 and 200 Pa. A deep minimum in the coefficient at 0.03–0.06 was observed and explained by a deposition of a rather smooth carbon film on the cobalt catalyst. Prolonged deposition caused the growth of perpendicularly oriented multilayer graphene sheets with the distance between the neighboring sheets around 100 nm. The large aspect ratio of the gaps, whose depth reached several micrometers after deposition time over 100 s, caused the trapping of oxygen atoms and, thus, numerous collisions with the graphene-like surface, so the coefficient increased for over an order of magnitude. The maximum coefficient over 0.5 was observed at low pressures and elevated temperatures. The evolution of the recombination coefficient was explained by the peculiarities of the binding sites for oxygen atoms on graphene surfaces.

1. Introduction

Neutral oxygen atoms play a crucial role in many advanced surface technologies, such as hydrophilization of polymeric materials [1], ashing of photo resistors [2], doping of graphene [3], and water decontamination [4]. A standard method for dissociating oxygen molecules at low temperatures is the application of non-equilibrium oxygen plasma [5]. Oxygen atoms are stable at low pressures since the conservation of energy and momentum at two-body collisions prevents association in the gas phase [6]. The loss of oxygen atoms in the gas phase by association of O atoms to parent molecules increases with increasing pressure because of the three-body collisions [7], where excessive potential energy before the collision is spent on the kinetic energy of molecules after the three-body collision. The collision frequency for three-body collisions increases as the square of the pressure [8], so the lifetime of short-lived radicals like atoms is of the order of μs at atmospheric pressure [9]. The loss of O-atoms in the reactors where plasma is sustained at low pressure is predominantly by surface recombination [10].

The heterogeneous surface association of atoms to stable molecules has attracted significant attention from the scientific community. Different surfaces exhibit various coefficients, and a review of the literature data was published recently [11]. The surface adsorption and association of O-atoms on graphite or graphene materials were studied in detail by several authors [12–15]. Moron et al. [16] provided detailed mechanisms of surface adsorption and recombination of O atoms on model graphite (0001) basal surface and found a moderate potential barrier of about 0.3 eV for surface adsorption of O atoms. The O atoms were preferentially bonded in the epoxy configuration (the bridge between 2 neighboring C atoms in the graphene plane). The recombination by the Eley-Rideal (ER) model was found to correspond to the perpendicular O – O orientation over the bridge site, while the Langmuir-Hinshelwood (LH) recombination involved a parallel position of the O-atoms. According to the ER model, the energy barrier for the recombination was found to be as low as 0.1 eV, while for the LH model, it was as high as 1.3 eV. The ER mechanism was found to be predominant in the range of temperatures from 300 to 900 K. The authors [16] stressed that

Abbreviations: CNW, carbon nanowalls; PECVD, plasma-enhanced chemical vapor deposition; ER, Eley-Rideal; LH, Langmuir-Hinshelwood; RF, radio frequency; SEM, scanning electron microscopy.

* Corresponding author.
E-mail address: domen.paul@ijs.si (D. Paul).

https://doi.org/10.1016/j.apsusc.2025.163654
Received 26 November 2024; Received in revised form 9 May 2025; Accepted 27 May 2025
Available online 27 May 2025

the calculated results were valid only for perfect graphite orientation and material without defects. The recombination coefficient was found to be between 10^{-5} and 3×10^{-4}. The maximum value was found at the temperature of about 600 K.

Cui et al. added the effect of chemical etching of graphite to their numerical code [17]. The etching rate increased with increasing temperature and became the predominant mechanism of the O-atom loss at temperatures above 900 K. They found the recombination coefficient independent from the graphite temperature up to about 900 K, but heating to higher temperatures caused a gradual coefficient decrease. They calculated the coefficient for heterogeneous surface recombination of O atoms to parent molecules as large as 0.3 in the range of graphite temperatures between 500 K and 700 K and gradual decrease at larger temperatures. The coefficient was about 0.1 at temperatures above 2000 K. The large coefficient calculated by Cui et al. code [17] as compared to Moron et al. [16] is explained by the structure of the graphite. While Moron et al. [16] took into account perfect monocrystals, the graphite examined by Cui et al. [17] was rich in defects, so it is feasible to conclude that the rough surface on the nanoscale enables much higher recombination coefficient.

Several authors also measured the recombination coefficient for graphite or graphene materials and reported various results. For example, Stewart [18] reported a gradual decrease in the recombination coefficient for carbon materials that are useful as heat-protecting shields for space vehicles in the range of temperatures between 1200 and 2000 K. The measurements were performed in the range of oxygen pressures between 500 and 3500 Pa, and the values were between 4×10^{-4} and 3×10^{-2}. Drenik et al. [19] deposited carbon films by sputter deposition in argon using a graphite target as a carbon source and reported a value of about 2×10^{-3} at room temperature in the oxygen pressure range of 30–280 Pa. Our team reported the largest coefficient for almost pure carbon in the form of perpendicularly oriented graphene sheets, with about 1 μm distance between neighboring sheets [20]. We measured the coefficient at a pressure of 50 Pa and found the value to be as large as 0.6. The perpendicularly oriented graphene sheets are also known as carbon nanowalls. One of the more recent and promising applications of carbon nanowalls is their use in solar cells [21–23], particularly in perovskite solar cells [24–26].

The brief literature survey reveals large discrepancies, which indicate that the coefficient for heterogeneous surface recombination of oxygen atoms on the carbon surfaces depends significantly on other parameters, including crystallinity and morphology. In the present paper, we report the evolution of the recombination coefficient for vertically oriented multilayer graphene sheets deposited on metal substrates by plasma-enhanced chemical vapor deposition using propane as the carbon precursor. The results explain the discrepancies between the above-cited authors. We used well-oxidized cobalt as the substrate for carbon deposits. The temperature and pressure dependence of the recombination coefficient for oxygen atoms on the cobalt surface (without carbon deposits) was studied in detail and reported in [27]. The coefficient in the range of temperatures between 300 and 800 K was between 0.05 and 0.3. The source of oxygen atoms was an early afterglow of inductively coupled oxygen plasma sustained in the H-mode. Details about the dissociation of oxygen molecules in such plasma were reported elsewhere [28]. Briefly, a coil connected to a radiofrequency generator provides the energy to dissociate the molecular oxygen in the system.

2. Experimental methods

Cobalt foils with a thickness of 0.05 mm and purity of 99.8 % were purchased from Goodfellow (United Kingdom). The foil was cut into discs with a diameter of 3 mm. The cobalt discs were spot-welded to chromel–alumel thermocouple wires (type K) with a diameter of 0.1 mm. They were well oxidized by exposure to inductively coupled oxygen plasma for a few minutes in order to obtain a stable oxide film of rich morphology. Such a treatment enables a stable recombination coefficient. Without the formation of the oxide film by exposure of the cobalt disc to oxygen plasma, an unpredictable growth of the oxide film would have occurred at elevated temperatures so that the recombination coefficient would have been dependent on the peculiarities of the previously performed experiments [27].

Thin films of vertically oriented multilayer graphene sheets were deposited on well-oxidized cobalt substrates using the experimental setup illustrated in Fig. 1 (a). The system was pumped with a two-stage rotary vane pump Edwards E2M80 (Edwards, United Kingdom) with a nominal pumping speed of 80 m^3/h. The system was hermetically tight, so the ultimate pressure, as measured with an absolute capacitive vacuum gauge Baratron 722A (MKS, USA), was below 1 Pa. A cobalt disc was placed into the discharge tube at the center of the radio frequency (RF) coil, as shown in Fig. 1 (a). The borosilicate discharge tube was 0.75 m long with outer/inner diameters of 4/3.6 cm. Before each series of measurements, the system was pumped for about 15 min to achieve the ultimate pressure; afterward, propane was introduced so that a stable pressure of about 17 Pa was achieved. The RF generator coupled to the RF coil via a matching network was set to the forward power of 500 W. The reflected power was between 5–20 W. A luminous plasma expanded in the volume within the RF coil at such conditions as illustrated in Fig. 1 (a). The volume of the luminous plasma, where coupling in the H-mode was achieved, was about 0.2 l, so the power density was as large as about 2500 W/l. Such a large power density enabled extensive dissociation of the propane precursor, as revealed by optical spectra (Fig. 2 (a)) and mass spectra (Fig. 2 (b)). The optical spectra were acquired with a wavelength-calibrated spectrometer (Avantes AviSpec-3648) and mass spectra with a differentially pumped mass residual gas analyzer (Pfeiffer Vacuum Prisma Pro QM6250). A typical temperature of the cobalt disc during the deposition of nanocarbon, as determined by the thermocouple, is shown in Fig. 2 (c).

The recombination coefficient was determined in the configuration, as shown in Fig. 1 (b). The cobalt disc with the nanocarbon deposits was moved away from the dense H-mode plasma to prevent extensive etching by reactive species from oxygen plasma (ions, metastables, and vacuum ultraviolet radiation) and overheating. According to Cui et al. [17], the etching becomes the predominant mechanism of the O-atom loss at temperatures above 900 K. The O-atom density at the position of the cobalt disc was measured with a calibrated catalytic probe (made by Plasmadis Ltd. in Ljubljana, Slovenia). The O-atom density at the position of the sample versus the oxygen pressure in the discharge tube is shown in Fig. 3 (a), with the discharge power as the parameter. A sharp drop in the O atom density for the curves measured at 200 and 300 W corresponds to the transition of the discharge mode from H- to E-mode, respectively.

A typical optical spectrum of oxygen plasma is shown in Fig. 3 (b). The spectrum consists of atomic lines because of the high dissociation fraction of O atoms and rather low electron temperature, which is typical for plasmas in the H-mode. The temperature of the cobalt sample with thick nanocarbon deposits increased during measurements of the recombination coefficient, and the typical temporal evolutions at a few pressures are shown in Fig. 3 (c) for the case of the discharge power of 500 W. The oxygen pressure is the parameter. The maximal achievable temperature at this discharge power is close to 800 K.

The recombination coefficient was determined by calorimetry. A cobalt disc with nanocarbon deposits was mounted into the discharge tube, as shown in Fig. 1 (b). The temperature of the cobalt disc was measured versus the exposure time to oxygen atoms. When the temperature stabilized, the oxygen plasma was turned off, and the time derivative of the temperature was measured. The recombination coefficient (γ) was determined as:

$$\gamma = \frac{8mc_p}{\bar{v}W_D Sn}\frac{dT}{dt}, \quad (1)$$

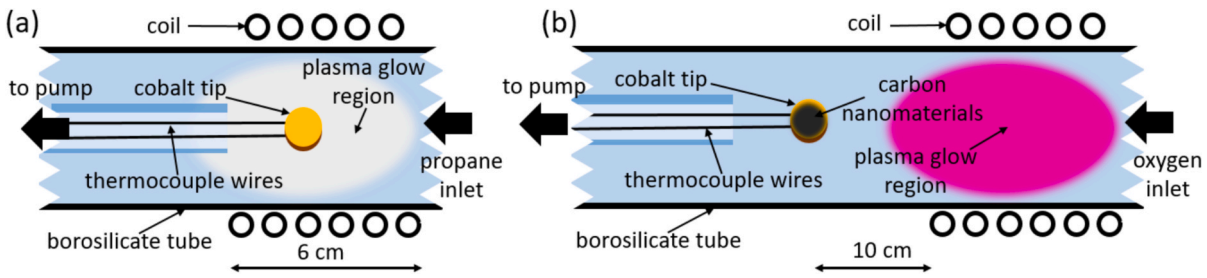

Fig. 1. Illustration of the discharge chamber and the position of the cobalt substrate during deposition of nanocarbon carbon by plasma-enhanced chemical vapor deposition (PECVD) (a) and when measuring the recombination coefficient (b). Propane inlet via a precise needle valve and oxygen inlet via a mass flow controller.

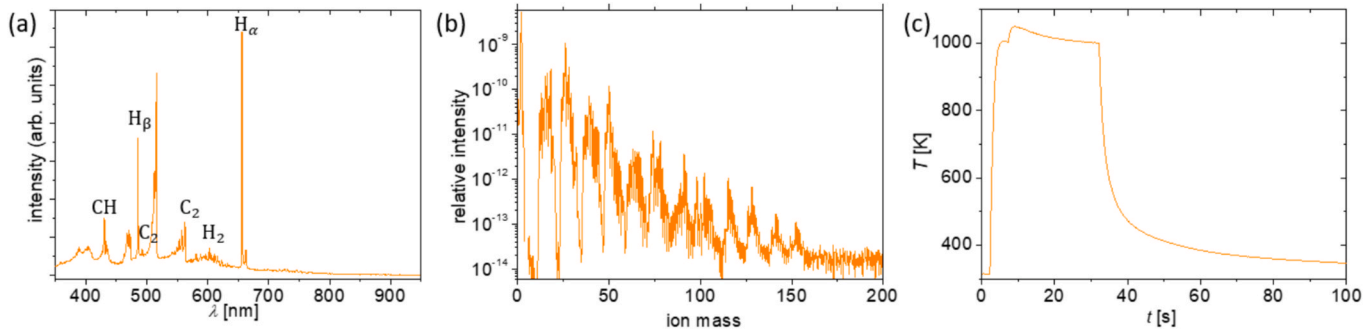

Fig. 2. Optical emission spectrum from propane plasma (a), mass spectrum of propane plasma (b), and the substrate temperature versus the treatment time during PECVD (c). Plasma was ignited at the time of 2 s and turned off at 32 s in (c).

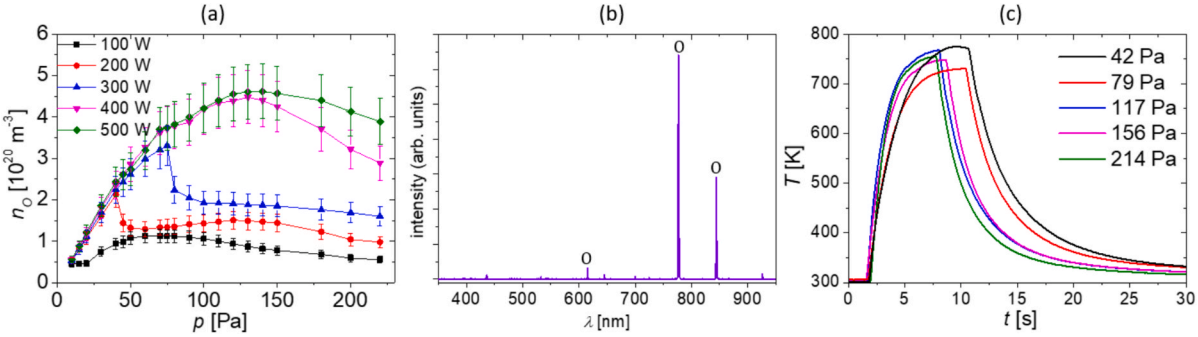

Fig. 3. The O-atom density at the position of the cobalt disc with nanocarbon deposits (a), optical emission from oxygen plasma at pressure 42 Pa and power 500 W (b), and the temperature of the cobalt disc versus the treatment time during measuring the recombination coefficient at maximum temperature of the probe tip and 5 different pressures (c). In Figure (c), plasma was ignited at $t = 2s$ and turned off between 10 and 15 s.

where m is the mass of the probe tip, c_p is the specific heat capacity of the probe tip, $\bar{v}$ is the average velocity of oxygen atoms, $W_D = 5.16$ eV is the dissociation energy of an oxygen molecule, S is the surface area of the probe tip, n is the neutral oxygen atom density at the position of the sample, and dT/dt is the first time derivative of the temperature of the probe tip.

The morphology of the carbon deposits on well-oxidized cobalt discs was determined by scanning electron microscopy (SEM), Verios 4G HP (Thermo Fisher, USA). It has a Schottky field emission electron gun with a monochromator. Samples were scanned at an accelerating voltage of 5 kV and current of 25 pA and were analyzed with an in-chamber Everhart-Thornley detector.

Additionally, the cross section of the sample was analyzed using transmission electron microscope (TEM), with special care taken in the preparation of the sample. The sample was gently mounted on a Si wafer from the outside, cut into a block, and mounted in a brass ring with epoxy glue. The TEM specimen was ground to a thickness of 100 μm and dimpled down to 15 μm at the disc center (Dimple grinder, Gatan Inc., Warrendale PA, USA). The TEM specimen was finally ion-milled (PIPS, Precision Ion Polishing System, Gatan Inc., USA) using 3 kV Ar^+ ions at an incidence angle of 8° until perforation.

Detailed investigations were performed using Spectra 300 (ThermoFisherScientific, Eindhoven, Netherlands) scanning transmission electron microscope (S/TEM) at an accelerating voltage of 200 kV. HRTEM images were captured with the Ceta M Camera to achieve high-quality atomic resolution through high-speed dynamic recording. STEM images were simultaneously recorded with a high-angle annular dark-field (HAADF) and a bright-field (BF) detector. The microscope is equipped with a Cs S-CORR probe corrector, a 4 x 30 mm^2 windowless Super-X EDS detector, an electron microscope pixel array detector (EMPAD), and a monochromator that, combined with the X-FEG gun and ultra-high stability, allows recording Electron Energy Loss Spectra (EELS) with high energy resolution.

3. Results and discussion

The nanocarbon deposits were prepared on numerous cobalt substrates (disks) using propane as the carbon precursor. The PECVD deposition times selected for this study ranged from 1 to 300 s. The cobalt discs were characterized by SEM after the deposition of nanocarbon. The evolution of the surface morphology is presented in SEM micrographs in Fig. 4. Images at other treatment times are available in the repository [29]. The SEM micrographs reveal rich morphology already for well-oxidized cobalt samples without a carbon deposit (Fig. 4 (a)). Such rich morphology is typical for many metal oxides and is the consequence of the oxidation in oxygen plasma at elevated temperatures [30,31]. The morphology is rich on the micrometer scale because the crystals in Fig. 4 (a) have a lateral dimension of around 1 μm.

A short 5-s treatment in propane plasma does not cause a significant change in the surface morphology on the micrometer scale, as revealed in Fig. 4 (b). The morphology on the micrometer scale is retained because the nanocarbon deposits are thin and fairly evenly deposited on the surface of the well-oxidized cobalt samples. Other morphological features are observed in Fig. 4 (b). The crystallites of cobalt oxides are covered with a thin film of carbon deposits, which grow on the substrate surface by thermal decomposition of the radicals formed in the propane plasma. According to Fig. 2 (a) and (b), the propane plasma is rich in various C_xH_y radicals. The radicals stick to the surface and decompose at the high surface temperature, which is close to 1000 K, as revealed in Fig. 2 (c). Gaps or pores between the neighboring grains of cobalt oxide are still observed in Fig. 4 (b) because the carbon deposits are thin. In Fig. 4 (c), after 15 s of deposition, a thin (and more even) layer of more developed nanostructures can be observed. The underlying cobalt oxide structures are still visible.

A significant change in the morphology happens after prolonged PECVD. Fig. 4 (d) reveals SEM micrographs of vertically oriented thin multilayer graphene sheets after depositing carbon for 30 s. The distance between the sheets is a few 100 nm. The exact growth mechanism is still not well understood, but the previous scientific reports confirmed that the carbon sheets consist of multilayer graphene flakes, often called carbon nanowalls [32–38]. Taking into account the rich composition of the plasma sustained in propane at the selected power (Fig. 2 (a) and (b)), it is clear that the mechanisms on the atomic scale will be difficult to explain by a theoretical model. Whatever the detailed mechanism, the vertically oriented nanocarbon covers the entire surface of the cobalt substrate after half a minute of PECVD time, as revealed in Fig. 4 (d).

The morphology of the carbon deposits is enriched after a prolonged deposition time, as shown in SEM micrographs (Fig. 4 (e) and (f)). It is not feasible to determine the thickness of the nanocarbon film on a substrate of such a rich morphology as our well-oxidized cobalt samples (Fig. 4 (a)), but the deposits can be peeled off the substrates after a prolonged PECVD process. Fig. 5 shows SEM micrographs of deposits scratched from the substrate after different deposition times. The height of the carbon deposit after a deposition time of 300 s (Fig. 5 (d)) is about 30 μm, and the deposit grows as columns from the surface of cobalt oxide crystallites. The width of the columns increases with the deposition time, and the columns eventually stick together to form a relatively continuous nanocarbon film, as revealed in Fig. 4 (f). We determined the thickness of the samples at selected PECVD times, shown on SEM micrographs (Fig. 5). We found a fairly linear increase, so the deposition rates are estimated to be several μm/min.

A TEM analysis was performed on the interface of carbon and cobalt oxide, as shown in Fig. 6 (a). Three areas of the sample were selected for a fast Fourier-transform (FFT) to determine the lattice constants: the first in the region of the oxidized cobalt (Fig. 6 (b)), the second in the interface region (Fig. 6 (c)), and the third in the region of carbon nanowalls (Fig. 6 (d)). As is visible from Fig. 6, only the first area was crystallinic, with lattice constants of 18.5 nm^{-1} and 7.92 nm^{-1}. This is in perfect agreement with Fig. 4, as the CNW layer is amorphous (Fig. 6 (d)), while the cobalt oxide underneath has a distinct crystallinic structure (Fig. 6 (b)). The FFT of the interface area (Fig. 6 (c)) is a mix of the other two areas, with blurry peaks, which points to a mix of a crystallinic and amorphous structures. Performing energy dispersive spectroscopy (EDS) on the samples, we identified the elements present in each of the three regions (Fig. 7 (a)). Plotting the atomic fractions of C, Co, and O in a linear profile across the interface region (Fig. 7 (b)) gives us a clearer picture of the interface region (Fig. 6 (c)): cobalt oxide is reduced, as observed by the lower fraction of oxygen and higher fraction of cobalt. From this, it is evident that a reduction of a thin layer of cobalt oxide on the surface of our metallic sample took place during the deposition process. The pure(er) cobalt along with the deposited carbon at the interface region exhibit a more amorphous structure than cobalt oxide while still retaining some crystallinity, explaining the FFT in Fig. 6 (c).

Numerous samples with carbon deposits were synthesized and installed separately into the system, as shown in Fig. 1 (b), to determine the recombination coefficient. As already mentioned, after a sample with a carbon deposit was placed into the reactor in Fig. 1 (b), the reactor was evacuated, oxygen at selected flow was leaked, and plasma was sustained at different pressures. We measured the recombination

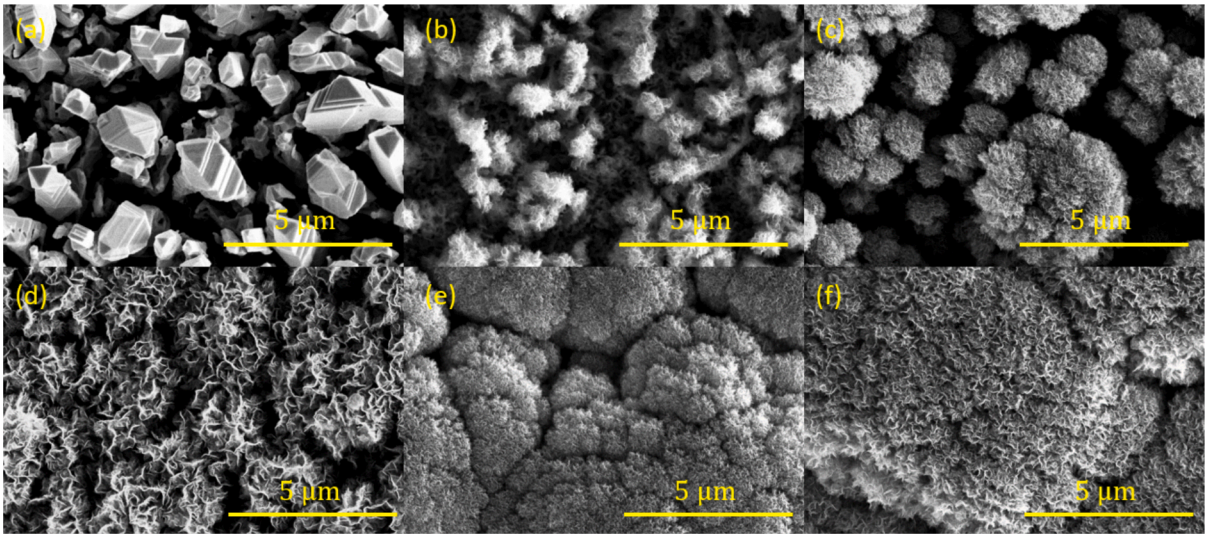

Fig. 4. SEM micrographs of the same magnification for the nanocarbon deposited on well-oxidized cobalt samples after PECVD for (a) 0, (b) 5, (c) 15, (d) 30, (e) 120, and (f) 300 s. The scale bar in all SEM micrographs is 5 μm.

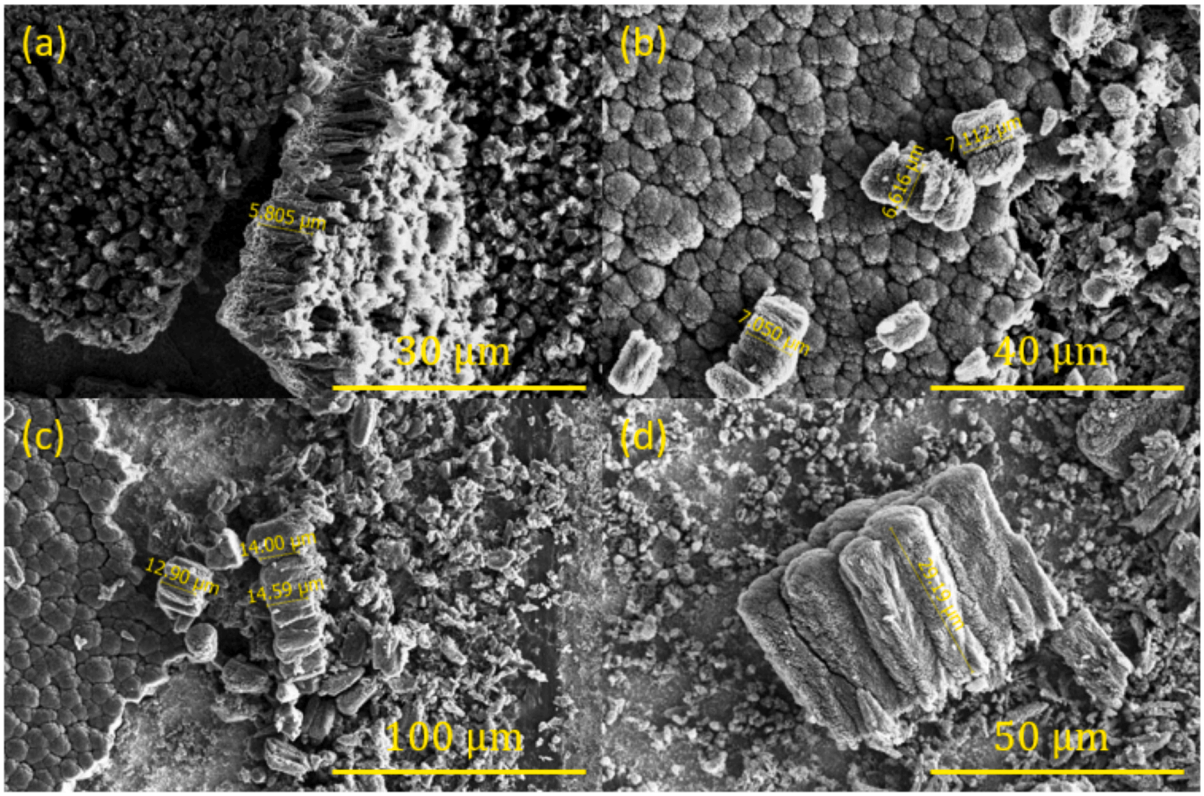

Fig. 5. SEM micrographs of CNW scratched off the surface of the cobalt oxide sample after 30 (a), 60 (b), 120 (c), and 300 (d) s deposition time. The thickness of the scratched-off layer increased rather linearly with increasing deposition time.

coefficients for samples with carbon deposits at the oxygen pressures of 42, 79, 117, 156, and 214 Pa, corresponding to oxygen flow of 250, 630, 1065, 1520, and 2240 cm, respectively. We selected the discharge powers for sustaining oxygen plasma of 500, 200, 100, 50, and 30 W. We measured the heating curves (as shown in Fig. 3 (c)) during exposure to the early afterglow of oxygen plasma and calculated the recombination coefficient according to Equation (1). The original measurements are in the repository [39].

Fig. 8 shows the evolution of the recombination coefficient for neutral oxygen atoms versus the deposition time of nanocarbon. Fig. 8 (a) reveals the recombination coefficient at the maximal achievable temperature of the samples. The maximal achievable temperature depends on the recombination coefficient because heterogeneous surface recombination is practically the only mechanism of the sample heating when placed at the position marked in Fig. 1 (b), i.e., 10 cm away from the dense oxygen plasma sustained in the H mode. The temperatures, of course, also depend on the density of O atoms in the vicinity of the sample installed into the system shown in Fig. 1 (b), and the O-atom density, in turn, depends on the discharge power and oxygen pressure in the system during the discharge. From this point of view, more representative are the curves in Fig. 8 (b), (c), and (d), which represent the recombination coefficient versus the nanocarbon deposition time at temperatures of 550, 450, and 350 K, respectively. Here, it is worth mentioning that these temperatures were not always achievable. For example, the temperature of 350 K was achieved practically for all samples, whereas 550 K was not achievable in the minimum of the curves at low pressures. The reason is that the heating by heterogeneous surface recombination was insufficient to enable such high temperatures in the case of low recombination coefficients.

All curves presented in Fig. 8 exhibit qualitatively the same behavior: the recombination coefficient is rather large for well-oxidized cobalt substrates (zero treatment time). The coefficient of cobalt depends on the pressure, and the reasons are explained in detail in the recent paper [27]. The coefficient also depends on the temperature of the well-oxidized cobalt surface.

Even a few seconds of treatment in propane plasma (configuration as in Fig. 1 (a)) causes a significant decrease in the recombination coefficient, as revealed in Fig. 8. A minimum appears in all curves in Fig. 8. The minimum appears for the samples treated with propane plasma for about 15 s. After that, the recombination coefficient increases and may reach the value already reported for perfectly vertically oriented multilayer graphene sheets [20], i.e., about 0.5. Interestingly enough, the pressure dependence of the recombination coefficient is well exhibited for very short or long deposition times. However, the pressure dependence is not so obvious in the range of deposition times, which corresponds to the minima in the curves in Fig. 8.

The appearance of the minimum in diagrams presented in Fig. 8 is worth discussing. As already mentioned, the recombination coefficient of perfectly smooth cobalt oxide and graphite is about 10^{-1} and 10^{-3}, respectively. In an approximation of perfectly smooth substrates and epitaxial growth of carbon in the form of a thin film, the recombination coefficient should be roughly 10^{-1} before depositing carbon and 10^{-3} after the entire cobalt surface has been covered with a monolayer of graphene. The hypothetical evolution of the recombination coefficient for such a (non-realistic, of course) case is illustrated in Fig. 9 (a). The recombination coefficient should decrease linearly with increasing coverage of the cobalt substrate with horizontally deposited graphene. Fig. 9 (a) is plotted in the lin-log scale, so the curve is not linear. Once the full coverage with a monolayer of horizontally oriented graphene is achieved, the recombination coefficient should stabilize at the value typical for perfectly smooth graphene, which is about 10^{-3} [16,18,19]. Fig. 9 (a) takes into account the perfectly smooth substrate surface and growth of carbon in the form of perfectly horizontal monolayers.

On the other hand, it is known that perfectly vertically oriented carbon nanowalls exhibit large recombination coefficients over 0.5 [20]. The hypothetical recombination coefficient for perfectly thin, vertically

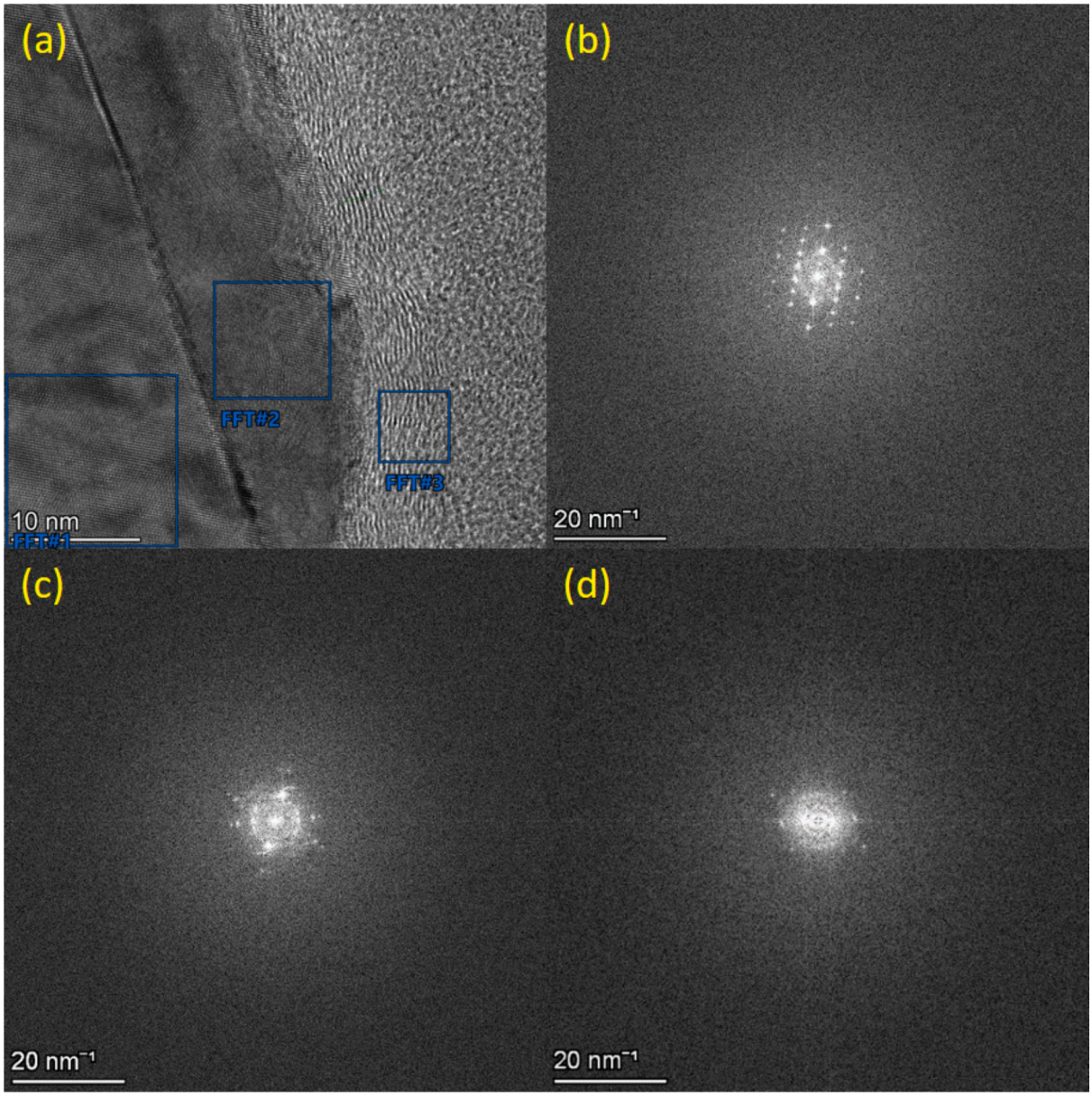

Fig. 6. HR-TEM image of the cross section of CNW deposited on an oxidized cobalt sample (a), where three regions were selected – the first in the cobalt oxide area, the second in the interface area, and the third in the CNW area. FFT diffraction patterns of the first (b), second (c), and third (d) are also shown.

oriented carbon nanowalls on the surface of perfectly smooth graphite is illustrated in Fig. 9 (b). In this approximation (not realistic either), the coefficient for the substrate without any vertical structure should be about 10^{-3}, the same as for the perfectly smooth cobalt fully covered with a perfectly smooth vertically oriented graphene. The coefficient will increase as soon as vertically oriented features appear on the surface of the perfectly smooth substrate and will increase with the increasing aspect ratio of the vertically oriented features. In the limited case, i.e., infinitely high vertical features of infinitely small thickness, the recombination coefficient will approach the theoretically maximal value, i.e., 1, because all atoms impinging such hypothetical structures will be trapped inside such a structure.

Taking into account the upper discussion and both illustrations in Fig. 9, the minimum in the measured curves presented in diagrams in Fig. 8 should be much deeper (recombination coefficient about 10^{-3}). Real materials behave differently, of course, and an explanation of the curves presented in Fig. 8 is provided as follows. Fig. 10 illustrates the growth of the nanocarbon films in the realistic scenario, i.e. using the substrates as disclosed in Fig. 4 (a). The well-oxidized cobalt surface (Fig. 10 (a)) exhibits a rich morphology on the micrometer scale, as also revealed by SEM micrographs in Fig. 4 (a). The surface is exposed to condensable radicals upon treatment with propane plasma and is partially depleted of O atoms by H radicals partly reducing the oxide layer, as observed in the TEM and EDS analysis (Figs. 6 and 7). The radicals will condense on the exposed cobalt surfaces, and very few will be able to penetrate deep into the micro gaps between the neighboring cobalt oxide columns, so the exposed surface will be covered with a thin film of nanocarbon. Still, the pores will remain almost free from nanocarbon deposits, as illustrated in Fig. 10 (b), because the radicals are lost by adsorption on the surfaces facing plasma and cannot reach the surface deep inside the gaps between the neighboring columns of cobalt oxide. The recombination coefficient in the range of treatment times in propane plasma up to about 15 s decreases monotonously with increasing deposition time because the area covered with carbon increases with increasing deposition time. As already explained in detail by Moron et al. [16] and confirmed experimentally by other authors [12–15 19],

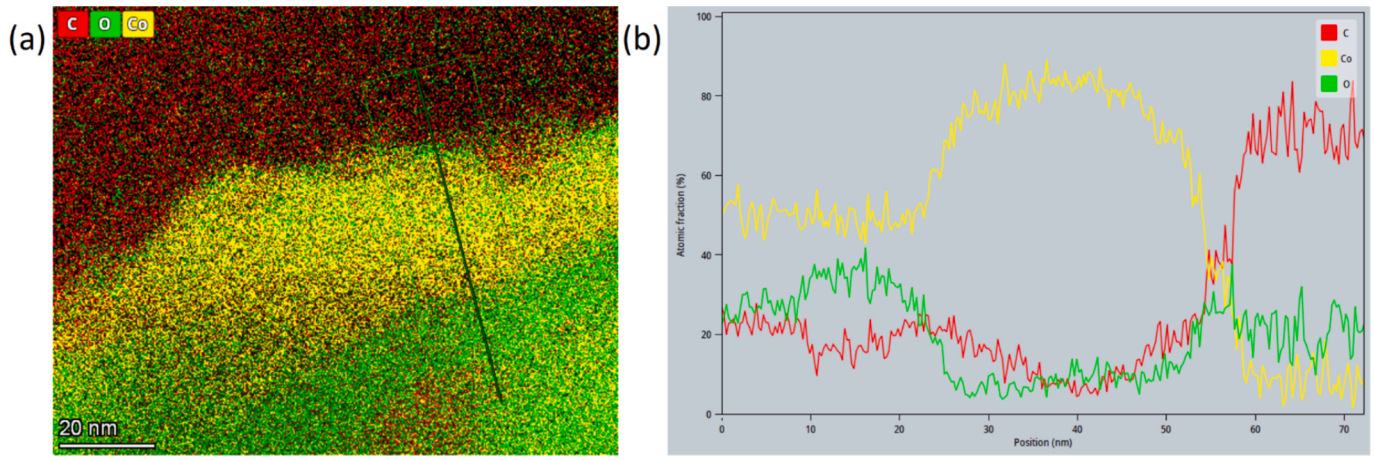

Fig. 7. EDS image of the interface region between the cobalt oxide and CNW (a), with a line crossing the interface. Atomic fractions of C, Co, and O taken from this linear profile are aslo shown (b).

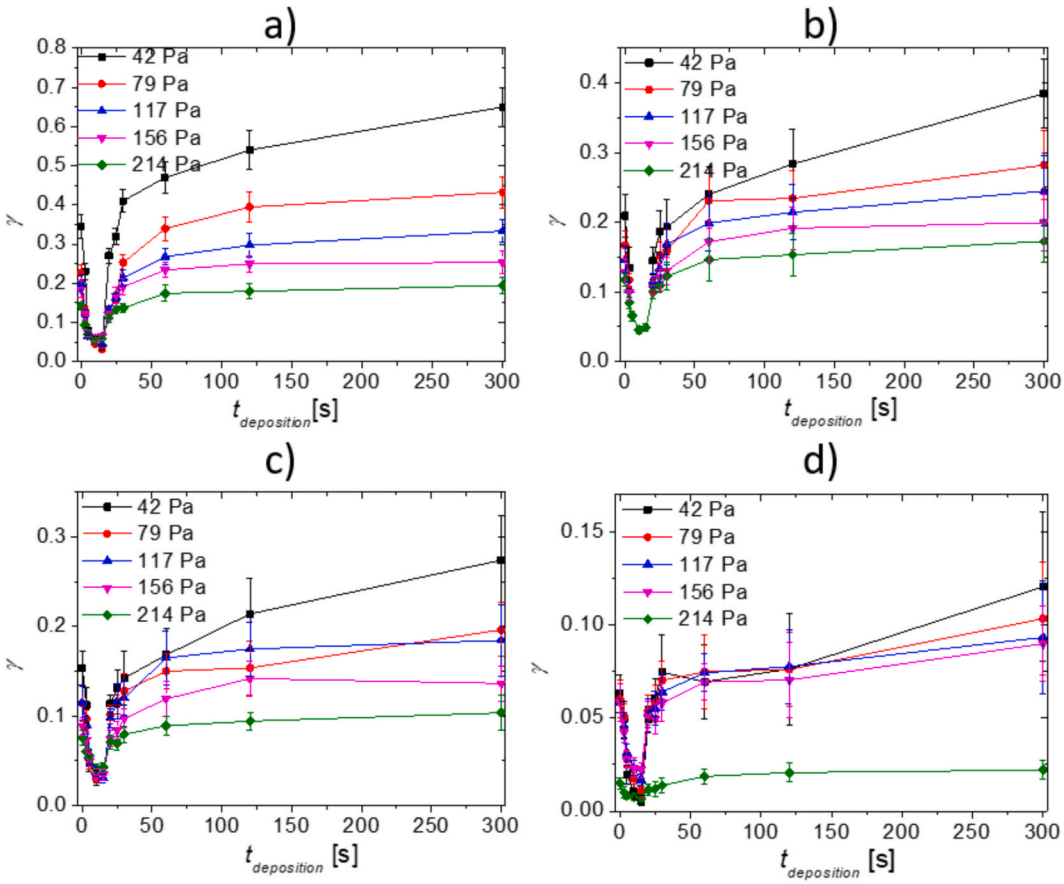

Fig. 8. The recombination coefficient for the surface association of oxygen atoms versus the deposition time in propane plasma: (a) at the maximal achievable temperature during exposure of the samples to the early afterglow of oxygen plasma; (b), (c), and (d) at the temperature of 550, 450, and 350 K, respectively. Achieving those temperatures was possible by varying the input power of the plasma generator.

graphene or graphite should exhibit a very low activity for heterogeneous surface recombination of oxygen atoms because of the limited concentration of the adsorption sites on the graphite surface as well as the rather large energy barrier of about 0.3 eV [16]. The appearance of the graphene-like material on the surface of the substrates should, therefore, cause a significant decrease in the recombination coefficient. However, the carbon deposits do not cover the entire surface, so a significant area is free from carbon deposits for short deposition times, as illustrated in Fig. 10 (b). The oxygen atoms impinging the surface after the initial growth of nanocarbon are, therefore, likely to hit the uncovered surface of cobalt oxide, where they recombine effectively, as shown in [27]. The recombination coefficient is thus moderate after short deposition times.

As the deposition time increases, a larger surface in the gaps between the columns of cobalt oxide becomes covered with carbon deposits. If the entire surface of cobalt oxide were covered with a thin film of carbon, the recombination coefficient should have dropped to the value typical for carbon deposits as obtained by sputter deposition, i.e., of the

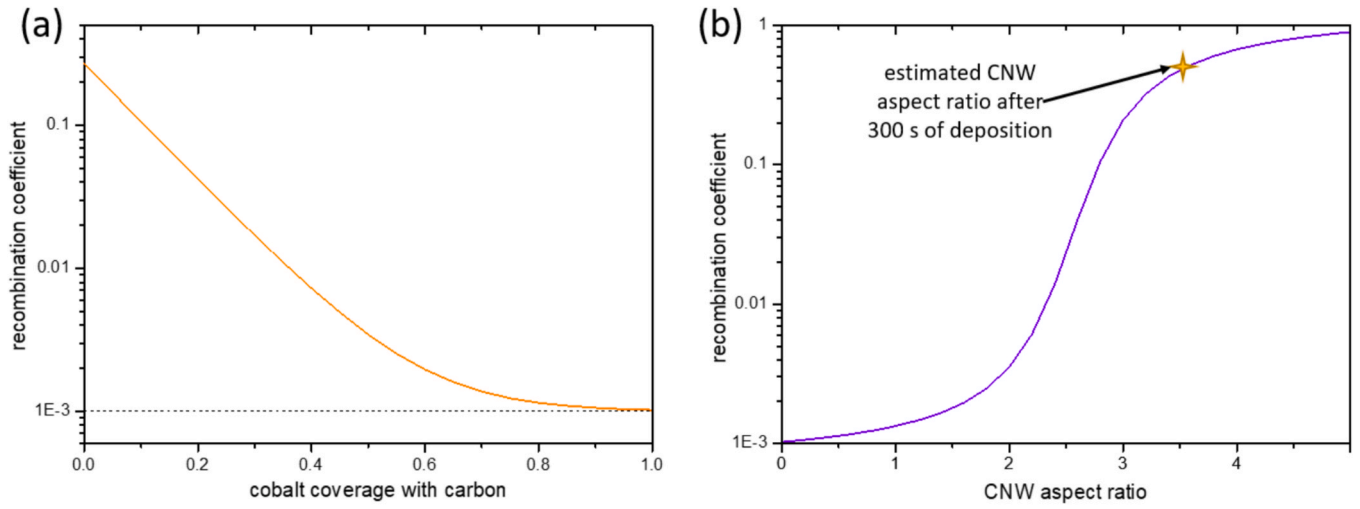

Fig. 9. The hypothetical dependence of the recombination coefficient for a perfectly smooth cobalt oxide surface versus the coverage of the surface with horizontally oriented graphene (a). The dependence of the coefficient for carbon nanowalls versus the aspect ratio of vertically oriented carbon nanowalls in the approximation of infinitely thin carbon nanowalls (b).

order of 10^{-3} [19]. The minima in the curves in Fig. 8, however, exhibit a moderate coefficient of the order of 10^{-2}. The paradox is explained by an evolution of the surface morphology of carbon deposits. Fig. 4 reveals structures that are often called carbon nanowalls [40–43]. Fig. 4 (d) shows thin nanowalls oriented perpendicularly on the surface of the cobalt oxide. The distance between the neighboring nanowalls is of the order of 100 nm. The nanowalls are high enough to cover the gaps between the neighboring cobalt oxide columns, so of the order of μm. The effect is illustrated in Fig. 10 (c). The oxygen atoms impinging the surface of the samples coated with the nanowalls will be trapped in the volume between the neighboring nanowalls because their mean free path at the pressures between 42 and 214 Pa is roughly 100 μm, orders of magnitude larger than the distance between the neighboring nanowalls. The O atoms will experience numerous collisions with the graphene-like surface. Although the loss coefficient at each collision is low [16], the considerable number of collisions makes the recombination coefficient large. The height of the nanowalls increases with increasing PECVD time, as does the number of collisions of O atoms in the gaps between neighboring nanowalls. This effect explains the rapid increase in the recombination coefficient in the range of deposition times between about 15 and 25 s (curves in Fig. 8).

More prolonged exposure of substrates to propane plasma causes densification of the nanocarbon deposits, as shown in Fig. 4 (f). The denser nanowalls and, thus, decreasing distance between two neighboring nanowalls cause a further increase in the recombination coefficient, as revealed in Fig. 8. The structure of the carbon deposits after prolonged deposition times using propane plasma is illustrated in Fig. 10 (d). The thickness of the deposits after the PECVD for 300 s was estimated by SEM (Fig. 5) after peeling off the nanowalls and was as large as about 30 μm. The distance between the neighboring nanowalls for the deposition time of 300 s is roughly 100 nm (Fig. 4 (f)), so the aspect ratio is very high. Few O atoms will escape from the gaps between the neighboring nanowalls, so the recombination coefficient becomes very large for such thick deposits.

The temperature dependence of the recombination coefficient is revealed in Fig. 11. The diagrams represent the measured coefficients versus the temperature of the cobalt substrates coated with the carbon deposits. Qualitatively, the behavior of the coefficient is the same for all experimental conditions: The coefficient increases monotonously with increasing sample temperature, and the minimal values are always observed for the samples exposed to propane plasma for about 15 s. This is due to two contradictory effects. At first, the recombination coefficient decreases, since the recombination coefficient of carbon is low. However, as the nanostructures begin to develop, impinging atoms can become trapped in the nanostructures, facilitating multiple collisions, and we can observe an increase in the recombination coefficient. The observed deposition time of 15 s represents the point where the effect of nanostructures entrapping the impinging atoms overtakes the effect of carbon's low recombination coefficient. The samples coated with thick carbon deposits (prolonged treatment time in the propane plasma) were heated extensively upon exposure to oxygen atoms in the system shown in Fig. 1 (b), so it was possible to measure the coefficient also at high temperatures up to about 800 K. This temperature is still low enough to prevent significant etching; hence, the samples remained visually intact even after exposure to O atoms at elevated temperatures. As shown by Cui et al [17], the significant etching of the carbon occurs only at temperatures above 900 K. Such large temperatures were not achievable in our system, even at large discharge powers.

Fig. 11 reveals a small coefficient, say between approximately 1 and 5×10^{-2} at the lowest achievable temperature, which was just above 300 K. Such low coefficients are sound with the experimental results reported by Drenik et al. [19], who performed the measurements at room temperature and found values as low as 2×10^{-3}. It is also sound with the calculation performed by Moron et al. [16]. The very low coefficient at the minimum in the curves plotted in Fig. 8 indicates that the thin carbon deposits represent a very weak drain of O atoms. This is in agreement with the general opinion that the O atoms bind strongly onto the graphene surface, so the interaction of the adatom with an atom from the gas phase is unlikely to occur. Moron et al. [16] calculated the coefficient as low as 2×10^{-6} at the oxygen pressure of 100 Pa and temperature of 300 K for perfect crystalline orientation. Our measurements presented in Fig. 11 provided larger coefficients, which may be explained by numerous defects in the deposited graphene structures. As mentioned above, Cui et al. [17] found much larger coefficients by considering the defects. Another feasible explanation for the coefficient between about 1 and 5×10^{-2} at a temperature just above 300 K could result in incomplete coverage of the catalytic substrate with carbon deposits, as illustrated in Fig. 10.

Elevated temperatures, above 400 K, were achievable in our experimental system for almost all samples. As revealed in Fig. 11, the coefficient increased monotonously with increasing temperature, which could be explained by either the E-R or L-H model. Since the L-H model predicts surface diffusion and association to form oxygen molecules with a moderate potential barrier, the increasing coefficient, as revealed in Fig. 11, is probably due to the L-H model. It should be stressed that the large potential barrier for an association of two adatoms reported by

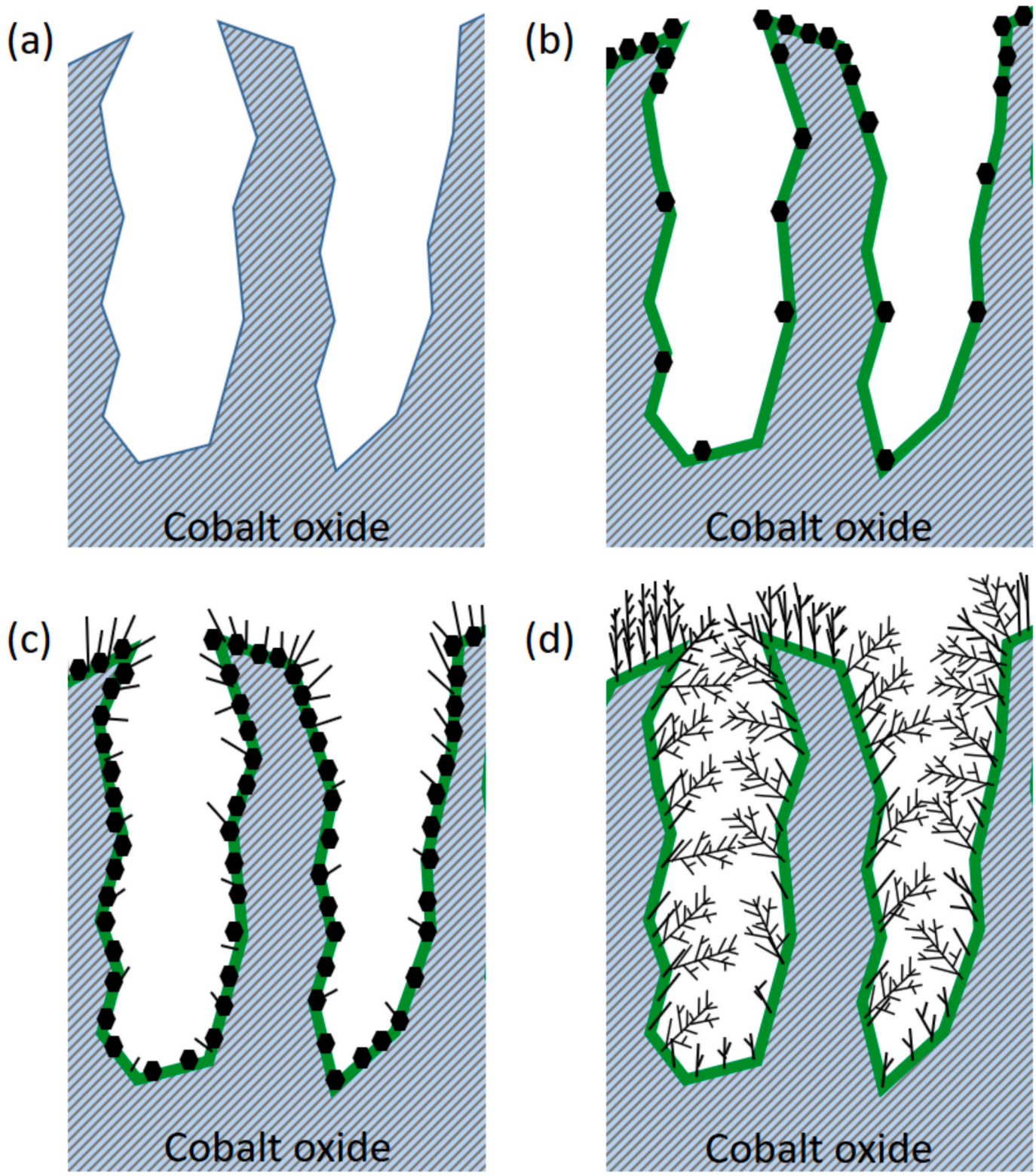

Fig. 10. The illustration of the formation of nanocarbon deposits upon PECVD in propane plasma. The well-oxidized cobalt surface exhibits a rich morphology on the micrometer scale (a). A short propane plasma treatment causes partial reduction of a thin oxide layer, shown as a green line, and a preferential carbon deposit growth on exposed areas (b). The deposition time of about 30 s enables the coating of the entire cobalt surface with multilayer graphene flakes (c). Long deposition times cause the formation of thick films of dense nanoflakes (d).

Moron et al. [16] is calculated for perfect crystal orientation, free from defects. The barrier should be much smaller in our case because carbon nanowalls, which grow at prolonged treatment times, are rich in defects [44–46]. A lower barrier for surface diffusion of adsorbed oxygen atoms will result in a higher probability for surface recombination of two adatoms by the Langmuir-Hinshelwood path [47].

Oxygen molecules will not chemisorb on the graphite surface, but there is a weak potential well for physisorption, as explained in the

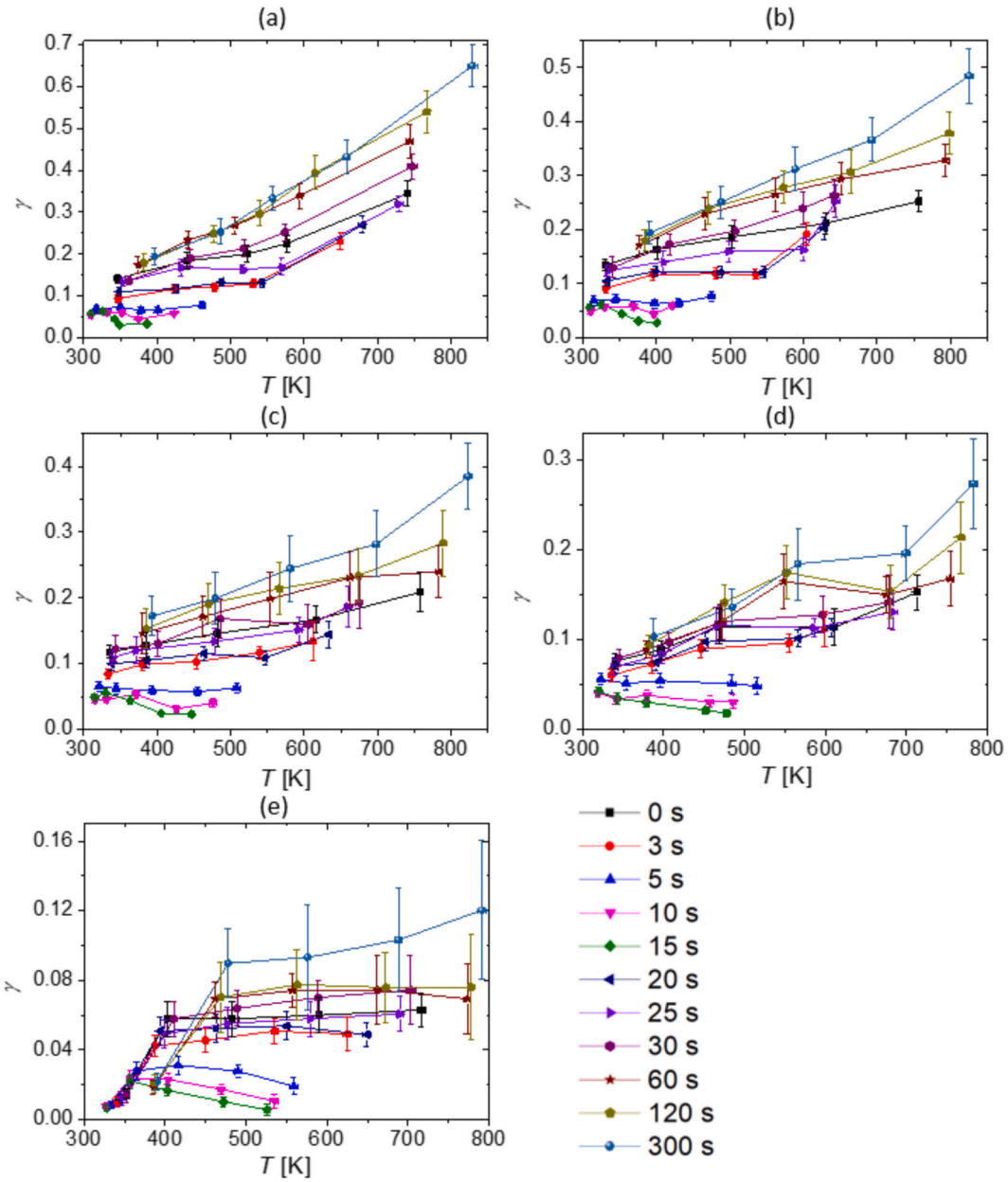

Fig. 11. The recombination coefficient for oxygen atoms on the surface of well-oxidized cobalt versus the sample temperature. The deposition time is the parameter. The coefficients are shown in diagrams (a), (b), (c), (d), and (e) for measurements performed at the oxygen pressure of 42, 79, 117, 156, and 214 Pa, respectively. The legend applies to all figures.

literature [48]. The surface density of physisorbed molecules will decrease with increasing temperature and increase with increasing pressure. The physisorbed molecules have a screening effect for binding sites of O atoms [49], so the recombination coefficient will likely increase with increasing temperature and decreasing pressure. The results summarized in Fig. 11 support the temperature dependence in the range of temperatures from 300 to 800 K and the pressure dependence at temperatures above about 400 K. Some deviations may be observed, especially for low coverage of oxidized cobalt with carbon, which is difficult to explain. It is worth mentioning that the accuracy of the catalytic probes for determining the density of oxygen atoms is about ± 20 %. The error bars shown in all diagrams, including Figs. 8 and 11, represent only the statistical error because we repeated the measurements several times. Adding the systematic error, the deviations observed for low coverages in Fig. 11 should be within the limits of the experimental error.

4. Conclusions

The coefficient for heterogeneous surface recombination of oxygen atoms on the nanocarbon was measured systematically in the range of O-atom flux of 7×10^{21} and 10^{23} $m^{-2}s^{-1}$, pressures between 42 and 214 Pa, and temperatures between 300 and 800 K. Nanocarbon was deposited on cobalt substrates using the PECVD method. As the nucleation of nanocarbon on the substrate occurs, the recombination coefficient starts decreasing because carbon exhibits a much lower coefficient for heterogeneous surface recombination of oxygen atoms than the oxidized cobalt substrate. With an increasing surface area of the substrate covered by carbon, the recombination coefficient decreases monotonously and reaches a value as low as 10^{-2}. Longer deposition times, which correspond to the thickness of the carbon film of a few 100 nm, cause the formation of carbon nanowalls. The oxygen atoms impinging the surface of such materials are trapped in the gaps between the

neighboring nanowalls and exhibit numerous collisions before escaping. Each collision provides a new chance for successful recombination, therefore multiple collisions lead to a higher recombination coefficient. Prolonged deposition times cause a larger aspect ratio of the gaps between neighboring carbon nanowalls, so the recombination coefficient keeps increasing with increasing deposition time. The maximum recombination coefficients of around 0.5 were measured for thick carbon deposits of rich morphology at high temperatures (above 700 K) and rather low pressures (42 Pa).

CRediT authorship contribution statement

Domen Paul: Writing – original draft, Visualization, Methodology, Formal analysis, Conceptualization. **Miran Mozetič:** Writing – review & editing, Writing – original draft, Supervision, Data curation, Conceptualization. **Gregor Primc:** Writing – review & editing, Visualization, Validation, Methodology, Investigation. **Alenka Vesel:** Writing – review & editing, Validation, Resources, Project administration, Funding acquisition. **Sandra Drev:** Investigation, Visualization. **Rok Zaplotnik:** Writing – review & editing, Validation, Supervision, Data curation.

Funding

This work was supported by the Slovenian Research and Innovation Agency, project L2-50052, titled Supercapacitors with graphene nanowalls, and core funding P2-0082, titled Thin-film structures and plasma surface Engineering.

Declaration of competing interest

The authors declare that they have no known competing financial interests or personal relationships that could have appeared to influence the work reported in this paper.

Data availability

Data has already been uploadet to repository, links provided in the article. https://doi.org/10.5281/zenodo.14203419 and https://doi.org/10.5281/zenodo.14203591

References

[1] P. Chytrosz-Wrobel, M. Golda-Cepa, E. Stodolak-Zych, J. Rysz, A. Kotarba, Effect of oxygen plasma-treatment on surface functional groups, wettability, and nanotopography features of medically relevant polymers with various crystallinities, Appl. Surf. Sci. Adv. 18 (2023).
[2] H.J. Jang, J.Y. Kim, E.Y. Jung, M. Choi, H.-S. Tae, Photoresist removal using reactive oxygen species produced by an atmospheric pressure plasma reactor, ECS J. Solid State Sci. Technol. 11 (2022).
[3] A. Ugartemendia, I. Casademont-Reig, L. Zhao, Z. Zhang, G. Frenking, J.M. Ugalde, A. Garcia-Lekue, E. Jimenez-Izal, Deciphering the chemical bonding of the trivalent oxygen atom in oxygen doped graphene, Chem. Sci., 15 (2024) 6151–6159.
[4] Y. Deng, Y.-X. Ye, Y. He, J. Xu, Z. Ke, X. Zhang, G. Ouyang, X. Yang, Highly effective activation of peroxymonosulfate via oxygen-coordinated single-atom iron for water decontamination, Chem. Eng. J. 485 (2024) 149782.
[5] H. Šourkova, P. Špatenka, Plasma activation of polyethylene powder, Polymers 12 (2020).
[6] E.J.H. Collart, J.A.G. Baggerman, R.J. Visser, Excitation mechanisms of oxygen atoms in a low pressure O2 radio-frequency plasma, J. Appl. Phys., 70 (1991) 5278–5281.
[7] L.D. Pietanza, Extended plateaux in the vibrational and electron distribution functions of O2/O reacting plasmas in discharge and post-discharge conditions, Phys. Plasmas 27 (2020).
[8] L. Tong, K. Saito, Three-dimensional simulation of a low-power microwave-excited microstrip plasma source, Jpn. J. Appl. Phys., 55 (2016).
[9] P. Attri, Y.H. Kim, D.H. Park, J.H. Park, Y.J. Hong, H.S. Uhm, K.-N. Kim, A. Fridman, E.H. Choi, Generation mechanism of hydroxyl radical species and its lifetime prediction during the plasma-initiated ultraviolet (UV) photolysis, Sci. Rep. 5 (2015).
[10] D.S. Hacker, S.A. Marshall, M. Steinberg, Recombination of atomic oxygen on surfaces, J. Chem. Phys., 35 (1961).
[11] D. Paul, M. Mozetič, R. Zaplotnik, G. Primc, D. Đonlagič, A. Vesel, "A review of recombination coefficients of neutral oxygen atoms for various materials," Materials, vol. 16, 2023.
[12] A. Incze, A. Pasturel, C. Chatillon, First-principles study of the atomic oxygen adsorption on the (0 0 0 1) graphite surface and dissolution, Appl. Surf. Sci. 177 (2001).
[13] D.C. Sorescu, K.D. Jordan, P. Avouris, Theoretical study of oxygen adsorption on graphite and the (8,0) single-walled carbon nanotube, J. Phys. Chem. B 105 (2001).
[14] J. Ito, J. Nakamura, A. Natori, Semiconducting nature of the oxygen-adsorbed graphene sheet, J. Appl. Phys., 103 (2008).
[15] Z. Xu, K. Xue, Engineering graphene by oxidation: a first-principles study, Nanotechnology 21 (2010).
[16] V. Moron, P. Gamallo, R. Sayos, DFT and kinetics study of O/O2 mixtures reacting over a graphite (0001) basal surface, Theor. Chem. Acc., 128 (2011).
[17] Z. Cui, J. Zhao, G. Yao, J. Zhang, Z. Li, Z. Tang, D. Wen, Competing effects of surface catalysis and ablation in hypersonic reentry aerothermodynamic environment, Chin. J. Aeronaut. 35 (2022).
[18] D.A. Stewart, Surface catalytic efficiency of advanced carbon carbon candidate thermal protection materials for SSTO vehicles, NASA Tech. Memo. 110383 (1996).
[19] A. Drenik, A. Vesel, M. Mozetič, P. Panjan, Recombination of atomic oxygen and hydrogen on amorphous carbon, J. Nucl. Mater. 442 (2013).
[20] M. Mozetič, A. Vesel, S.D. Stoica, S. Vizireanu, G. Dinescu, R. Zaplotnik, Oxygen atom loss coefficient of carbon nanowalls, Appl. Surf. Sci. 333 (2015).
[21] L. Liu, L. Jia, Y. Huang, Y. Zhang, W. Yu, High-performance vertical graphene nanowall/silicon Schottky junction solar cells with Nafion doping and plasma etching, J. Alloy. Compd. 939 (2023) 168765.
[22] W. Maiaugree, A. Tangtrakarn, S. Lowpa, N. Ratchapolthavisin, V. Amornkitbamrung, Facile synthesis of bilayer carbon/Ni3S2 nanowalls for a counter electrode of dye-sensitized solar cell, Electrochemica Acta 174 (2015) 955–962.
[23] M. Eryigit, S. Mobtakeri, E.P. Gur, E. Temur, T.O. Ozer, U. Demir, E. Gur, Efficient CdS quantum dot sensitized solar cells based on electrochemically reduced graphene oxide (ERGO)/ZnO nanowall photoanodes and MoS2, WS2, CuS cascaded counter electrodes, Sol. Energy 234 (2022) 348–359.
[24] M. Yang, H. Wang, W. Cai, Z. Zang, Mixed-halide inorganic perovskite solar cells: opportunities and challenges, Adv. Opt. Mater. 11 (2023) 2301052.
[25] Y. Zhou, Z. Guo, S.M.H. Qaid, Z. Xu, Y. Zhou, Z. Zang, Strain engineering toward high-performance formamidinium-based perovskite solar cells, Sol. RRL 7 (2023) 2300438.
[26] Z. Zang, S. Zhao, W. Cai, H. Wang, "Inorganic Perovskite Solar Cells," in Inorganic Perovskite Materials and Devices, Singapore, Springer Nature Singapore Pte Ltd., (2024) 171–203.
[27] D. Paul, M. Mozetič, R. Zaplotnik, J. Ekar, A. Vesel, G. Primc, D. Đonlagič, Loss of oxygen atoms on well-oxidized cobalt by heterogeneous surface recombination, Materials 16 (2023).
[28] R. Zaplotnik, A. Vesel, M. Mozetič, Transition from E to H mode in inductively coupled oxygen plasma: Hysteresis and the behavior of oxygen atom density, Europhys. Lett. 95 (2011).
[29] D. Paul, M. Mozetič, G. Primc, A. Vesel, R. Zaplontik, SEM images of CNW on oxidized Co sample, 22 11 2024. [Online]. Available: doi.org/10.5281/zenodo.14203419.
[30] S. Thangabalu, N. Senthil Kumar, T. Usha Devi, S. Selvi, J.H. Chang, K. Mohanraj, Impact of substrate temperature on the properties of yttrium oxide thin films prepared by nebulizer spray pyrolysis technique, Materials Today: Proceedings 48 (2022) 229-233.
[31] G. Zhou, J.C. Yang, Temperature effect on the Cu 2O oxide morphology created by oxidation of Cu(0 0 1) as investigated by in situ UHV TEM, Appl. Surf. Sci. 210 (2003) 165–170.
[32] A. Reguig, B. Vishal, J. Smajic, M. Bahabri, G. Deokar, M.A. Alrefae, P.M.F.J. Costa, Graphene nanowalls grown on copper mesh, Nanotechnology 35 (2023).
[33] B. Vishal, A. Reguig, M. Bagabri, P.M.F.J. Costa, Graphene nanowalls formation investigated by electron energy loss spectroscopy, Sci. Rep. 14 (2024).
[34] Z. Wu, E. Wang, G. Zhang, Y. Shen, G. Shao, Recent progress of vertical graphene: preparation, structure engineering, and emerging energy applications, Small 20 (2024).
[35] A. Jagodar, N.M. Santhosh, T. Strunskus, E. von Wahl, A. Petit, T. Lecas, M. Košiček, U. Cvelbar, J. Berndt, E. Kovacevic, Growth of graphene nanowalls in low-temperature plasma: Experimental insight in initial growth and importance of wall conditioning, Appl. Surf. Sci. 643 (2024).
[36] K. Kim, C.Y. Bon, J. Kim, J.M. Ko, W. Choi, Carbon nanowalls as anode materials with improved performance using carbon nanofibers, Nanomaterials 13 (2023).
[37] T.-T. Zhang, B.-H. Lv, C.-C. Fan, B.-Y. Shi, Q.-J. Cao, W. Wang, F.-F. Tao, W.-D. Dou, Controllable fabrication of vertical graphene with tunable growth nature by remote plasma-enhanced chemical vapor deposition, ACS Omega 8 (2023).
[38] E. Bertram-Serra, S. Rodriguez-Miguel, Z. Li, Y. Ma, G. Farid, S. Chaitoglou, R. Amade, R. Ospina, J.-L. Andujar, Advancements in plasma-enhanced chemical vapor deposition for producing vertical graphene nanowalls, Nanomaterials 13 (2023).
[39] D. Paul, M. Mozetic, G. Primc, A. Vesel and R. Zaplotnik, "Heating curves of catalytic probe with cobalt tip and varying thicknesses of carbon nanowall deposition in oxygen plasma," 22 11 2024. [Online]. Available: doi.org/10.5281/zenodo.14203591.
[40] Y. Wu, P. Qiao, T. Chong, Z. Shen, Carbon nanowalls grown by microwave plasma enhanced chemical vapor deposition, Adv. Mater. 14 (2002) 64–67.

[41] Y. Wu, B. Yang, B. Zong, H. Sun, Z. Shen, Y. Feng, Carbon nanowalls and related materials, J. Mater. Chem., 14 (2004) 469–477.
[42] M. Hiramatsu, K. Shiji, H. Amano, M. Hori, Fabrication of vertically aligned carbon nanowalls using capacitively coupled plasma-enhanced chemical vapor deposition assisted by hydrogen radical injection, Appl. Phys. Lett., 84 (23) (2004) 4708–4710.
[43] K. Shiji, M. Hiramatsu, A. Enomoto, M. Nakamura, H. Amano, M. Hori, Vertical growth of carbon nanowalls using rf plasma-enhanced chemical vapor deposition, Diamon & Related Materials 14 (2005) 831–834.
[44] Z.H. Ni, H.M. Fan, X.F. Fan, H.M. Wang, Z. Zheng, Y.P. Feng, Y.H. Wu, Z.X. Shen, High temperature Raman spectroscopy studies of carbon nanowalls, J. Raman Spectrosc. 38 (2007) 1449–1453.
[45] N.V. Suetin, S.A. Evlashin, A.V. Egorov, K.V. Mironovich, S.A. Dagesyan, L. V. Yashina, E.A. Goodilin, V.A. Krivchenko, Self-assembled nanoparticle patterns on carbon nanowall surfaces, Phys. Chem. Chem. Phys., 18 (2016) 12344–12349.
[46] D.G. Batryshev, Y. Yerlanuly, T.S. Ramazanov, M.K. Dosbolayev, M.T. Gabdullin, Elaboration of carbon nanowalls using radio frequency plasma enhanced chemical vapor deposition, Mater. Today Proc. 5 (2018) 22764–22769.
[47] S.N. Mikhailov, L.C.A. van den Oetelaar, H.H. Brongersma, R.A. van Santen, Oxidation of carbidic carbon on a rhodium surface, Catal. Lett. 27 (1994) 79–90.
[48] D. Lamoen, B.N.J. Persson, Adsorption of potassium and oxygen on graphite: A theoretical study, J. Chem. Phys., 108 (1998) 3332–3341.
[49] J.-P. Booth, O. Guaitella, A. Chatterjee, C. Drag, V. Guerra, D. Lopaev, S. Zyryanov, T. Rakhimova, D. Voloshin, Y. Mankelevich, Oxygen (3P) atom recombination on a pyrex surface in an O2 plasma, Plasma Sources Sci. Technol., 28 (2019) 055005.